Check for updates

ORIGINAL PAPER

physica status solidi b

www.pss-b.com

Optical–Microwave Pump–Probe Studies of Electronic Properties in Novel Materials

*Sándor Kollarics, András Bojtor, Kristóf Koltai, Bence Gábor Márkus, Károly Holczer, János Volk, Gergely Klujber, Máté Szieberth, and Ferenc Simon**

Combined microwave–optical pump–probe methods are emerging to study the quantum state of spin qubit centers and the charge dynamics in semiconductors. A major hindrance is the limited bandwidth of microwave irradiation/detection circuitry which can be overcome with the use of broadband coplanar waveguides (CPWs). The development and performance characterization of two spectrometers is presented as follows: an optically detected magnetic resonance spectrometer (ODMR) and a microwave-detected photoconductivity measurement. In the first method, light serves as detection and microwaves excite the investigated medium, whereas in the second, the roles are interchanged. The performance is demonstrated by measuring ODMR maps on the nitrogen-vacancy (NV) center in diamond and time-resolved photoconductivity in *p*-doped silicon. The results demonstrate both an efficient coupling of the microwave irradiation to the samples as well as an excellent sensitivity for minute changes in sample conductivity.

1. Introduction

Optical pump–probe spectroscopy and microscopy experiments represent an important branch of tools to study the conduction dynamics in novel materials[1] or nonequilibrium states.[2] Alternatively, electromagnetic radiation with very different wavelength can be combined in a similar pump–probe way, which enables to study physical phenomena occurring on the different energy scales. The combined microwave–optical pump–probe methods enable, for example, to detect microwave-induced spin transitions with optics, a method known as optically detected magnetic resonance (ODMR). The reverse situation occurs in microwave-detected photoconductivity decay (μ-PCD), where optically induced nonequilibrium charge carriers cause a change in the reflected microwave intensity, thus enabling a study of charge recombination in a time-resolved manner.

ODMR[3] spectroscopy is a powerful tool to study the spin states of novel systems such as carbon nanotubes,[4] fullerenes,[5] and nitrogen-vacancy (NV) centers in diamond[6] for applications in spintronics,[7] quantum computing,[8] or light-emitting diodes.[9] This technique benefits from the high energy resolution of the microwaves (down to a few 100 kHz, i.e., neV energy range) with the high efficiency of optical photon detection. It is even possible to detect the change in luminescence of a single molecule.[10]

μ-PCD measurement[11] is widely used in semiconductor industry to study the impurity concentration in silicon wafers[12] or nonsilicon semiconductors such as CdTe.[13] This contactless method enables manufacturers to determine impurity concentrations with great accuracy and researchers to gain information on charge carrier dynamics on the nanosecond timescale.

A key element of the instruments in both cases is the microwave irradiation unit, which is most often a resonator, offering a high microwave power to electric or magnetic field conversion due to the resonator quality factor, at the cost of a reduced bandwidth. Alternatively, microwave antennas[14] are often used but these have

S. Kollarics, A. Bojtor, K. Koltai, B. G. Márkus, Prof. F. Simon
Department of Physics
MTA-BME Lendület Spintronics Research Group (PROSPIN)
Budapest University of Technology and Economics
P.O. Box 91, H-1521 Budapest, Hungary
E-mail: f.simon@eik.bme.hu

Prof. K. Holczer
Department of Physics and Astronomy
UCLA
Los Angeles, CA 90095-1547, USA

The ORCID identification number(s) for the author(s) of this article can be found under https://doi.org/10.1002/pssb.202000298.

© 2020 The Authors. Published by Wiley-VCH GmbH. This is an open access article under the terms of the Creative Commons Attribution License, which permits use, distribution and reproduction in any medium, provided the original work is properly cited.

DOI: 10.1002/pssb.202000298

Dr. J. Volk
Centre for Energy Research
Institute of Technical Physics and Materials Science
Konkoly-Thege M. út 29-33, Budapest 1121, Hungary

G. Klujber, Dr. M. Szieberth
Institute of Nuclear Techniques
Budapest University of Technology and Economics
Műegyetem rkp. 9, H-1111 Budapest, Hungary

S. Kollarics, B. G. Márkus, Prof. F. Simon
Laboratory of Physics of Complex Matter
École Polytechnique Fédérale de Lausanne
Lausanne CH-1015, Switzerland

usually smaller bandwidth and worse microwave power to magnetic field conversion ratio. In principle compact, nonresonant waveguides combine both the large bandwidth with the good filling factor, which results in an excellent microwave power to magnetic field conversion. Coplanar waveguides (CPWs)[15,16] and slot lines[17] consist of metallic lines placed on high dielectric constant substrates. This layout confines the microwave fields traveling in a quasi-TEM (transverse electromagnetic) mode[18] to a small volume giving a huge electromagnetic energy density competing with classical resonators. These miniaturized waveguides can be combined with surface mount devices (SMDs)[19] and other circuit elements. CPWs also opened a way toward microwave device miniaturization such as production of millimeter-scale circulators.[20]

In case of resonators, the access to the sample such as optical illumination or application of external electric field is limited and it affects the performance of the resonator, e.g., a window on the wall of the resonator lowers the *Q*-factor. The broadband operation of CPWs makes frequency swept experiments such as permeability measurement[21] and ferromagnetic resonance studies[22] also very effective.

In this article, we present the development and performance characterization of two instruments, which both operate with CPWs. We present a broadband ODMR spectrometer which allowed to study quantum states of NV centers in diamond. The μ-PCD instrument has a good sensitivity for small changes in sample conductivity during the transient decay of the charge carriers.

2. The Spectrometer Setups

2.1. The ODMR Spectrometer

The setup of the ODMR spectrometer is shown in **Figure 1**. The CPW holding the sample is illuminated using a continuous wave laser (532 nm Coherent Verdi 5G frequency-doubled Nd:YAG). The luminescent light is collected and focused by the so-called "image relay" consisting of an achromatic doublet pair (Thorlabs MAP1030100-B) to a spectrograph (Horiba JY iHR320) equipped with a photomultiplier tube (Hamamatsu R2658P) and a single-pixel InGaAs detector (Horiba DSS-IGA010L). The former covers

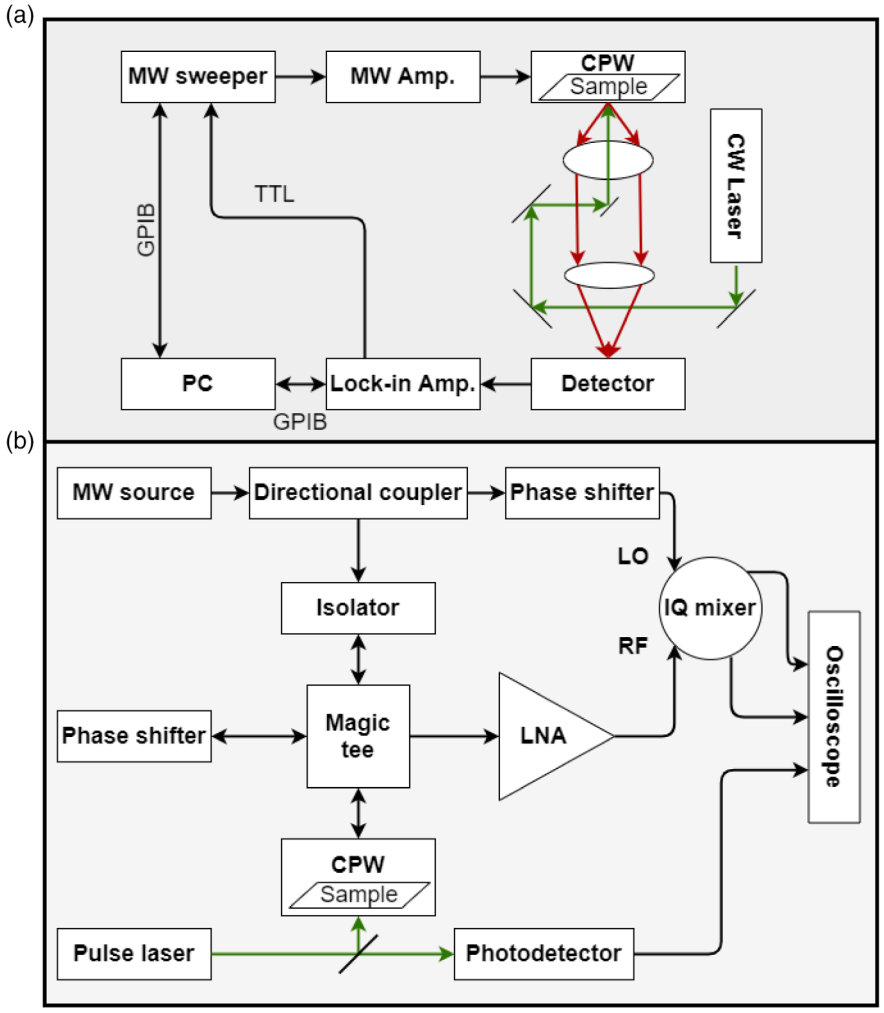

Figure 1. a) Block diagram of the ODMR setup and b) the μ-PCD setup. Passive attenuators and DC blocks are not shown to retain clarity.

© 2020 The Authors. Published by Wiley-VCH GmbH

15213951, 2020, 12, Downloaded from https://onlinelibrary.wiley.com/doi/10.1002/pssb.202000298 by Cochrane Germany, Wiley Online Library on [02/12/2023]. See the Terms and Conditions (https://onlinelibrary.wiley.com/terms-and-conditions) on Wiley Online Library for rules of use; OA articles are governed by the applicable Creative Commons License

the ultraviolet (UV) to near infrared (NIR) range (185–1010 nm), whereas the latter is optimized for the NIR range (1000–1900 nm). The detector output is connected to a lock-in amplifier (Stanford Research Systems, SR830) through a transimpedance amplifier. The output of the microwave signal generator (HP83751B) is chopped by the TTL (transistor–transistor logic) signal coming from the lock-in amplifier. The microwaves are fed into an amplifier (Kuhne KuPa 270330-10A, Gain = 40 dB) and then sent to the CPW which has a 50 Ω termination at its end. The CPW is placed on a two-axis miniature dovetail translation stage (Thorlabs DT12XY/M) during room temperature measurements. To apply external magnetic field, the stage and the other optics parts are placed on a rail that can be rolled into the middle of an electromagnet with a magnetic field up to 1.2 T.

2.2. The μ-PCD Spectrometer

Figure 1 shows the μ-PCD measurement setup which is a modification of our previous resonator-based, time resolved μ-PCD setup described elsewhere.[23] A Q-switch pulsed laser (527 nm Coherent Evolution-15, frequency-doubled Nd:YLF) with a 1 kHz repetition rate, pulse energy of 150 μJ, and a pulse width of 1.7 μs is used for excitation of charge carriers in the sample placed on the CPW.

The microwave oscillator (Kuhne MKU LO 8-13 PLL) serves as the source of the probing microwave (MW) field and as the local oscillator of a double-balanced in-phase quadrature (IQ) mixer. The directional coupler sends half of the incoming power through an isolator (to avoid damage of the oscillator unit by reflected power) to the magic tee, and the other half drives the IQ mixer. Half of the incoming microwave power is directed toward the CPW, and the other half to the port with a phase-shifter and a variable attenuator attached. The waves reflected from the CPW and the other port interfere with each other on the fourth port allowing us to get rid off the DC reflection by setting the attenuation and phase properly. The previously described MW bridge is followed by a low-noise amplifier (JaniLab Inc. Gain = 15 dB) and the amplified signal is fed to the IQ mixer. The I (in-phase) and Q (quadrature) signals down-converted from the detected RF signal are digitized with an oscilloscope (Tektronix MDO-3024, BW = 200 MHz) which is triggered by the signal coming from the photodetector (Thorlabs DET36A/M) sensing the laser pulse.

2.3. The Cryostat

To conduct cryogenic measurement, we built a closed cylindrical compartment with optical access through a quartz window (Ø1″) and MW connection using an UHV SMA (ultra-high vacuum SubMiniature version A) connector. The CPW is fixed to a copper cube attached to the inner tube that can be filled with liquid nitrogen from the outside. The space between the two tubes where the CPW is placed is evacuated using a turbomolecular pump (Pfeiffer HiCube Eco). Vacuum level of 10^{-6} mbar is easily achievable and grants long enough measurement time without any condensation problems on the outside or heating of the sample.

2.4. Samples

ODMR measurements were performed on single crystal (3 × 3 × 0.3 mm) type-Ib diamond samples (Element Six Ltd.) produced by high pressure high temperature method (HPHT), containing less than 200 ppm substitutional nitrogen. After neutron irradiation of the diamond plates in the Training Reactor of the Institute of Nuclear Techniques (located at the Budapest University of Technology and Economics) for 8 h at 100 kW power with a total fluence of $\approx 10^{17}$ cm^{-2} (3×10^{16} cm^{-2} in the 100 eV–1 MeV range), the samples were annealed under dynamic vacuum (10^{-5} mbar) at 800–1000 °C to help the diffusion of vacancies creating the NV centers. To dissolve surface contamination, samples were put into vials containing a mixture of acetone and isopropyl alcohol and bath sonicated for 15 min.

μ-PCD measurements were conducted on phosphorus-doped silicon wafer with an approximate surface of 10 mm^2 and a thickness of 200 μm. The resistivity of the sample was 0.528 Ω·cm, as determined by a four-point sheet resistivity measurement technique.

3. Spectrometer Characterization

3.1. ODMR on NV Centers in Diamond

In this article, we present a range of measurements to demonstrate the versatile applicability of CPWs. First, ODMR measurements in variable external magnetic fields are shown along with a wavelength-resolved zero field ODMR map. We conducted ODMR measurements on diamond samples to demonstrate the advantages of applying CPWs for MW irradiation. **Figure 2** shows microwave frequency sweeps performed in zero magnetic field and also in 5 mT.

These spectra were acquired in a constant external magnetic field, whereas the microwave frequency was swept and chopped by the TTL signal of the lock-in amplifier. **Figure 3** on the other hand shows a magnetic field sweep at a constant microwave frequency of 9.2 GHz. Here, the MW amplifier was replaced with one working in the X-band (Kuhne KuPa 9001250-2A,

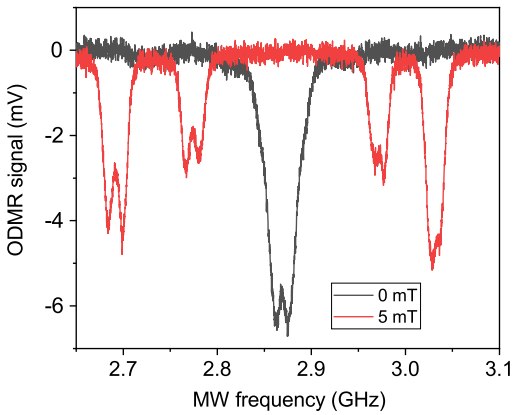

Figure 2. ODMR on NV centers in diamond detected at 680 nm. In zero magnetic field (black line), the resonances are degenerate, whereas applying external magnetic field of 5 mT (red line) resolves the degeneracy.

© 2020 The Authors. Published by Wiley-VCH GmbH

15213951, 2020, 12, Downloaded from https://onlinelibrary.wiley.com/doi/10.1002/pssb.202000298 by Cochrane Germany, Wiley Online Library on [02/12/2023]. See the Terms and Conditions (https://onlinelibrary.wiley.com/terms-and-conditions) on Wiley Online Library for rules of use; OA articles are governed by the applicable Creative Commons License

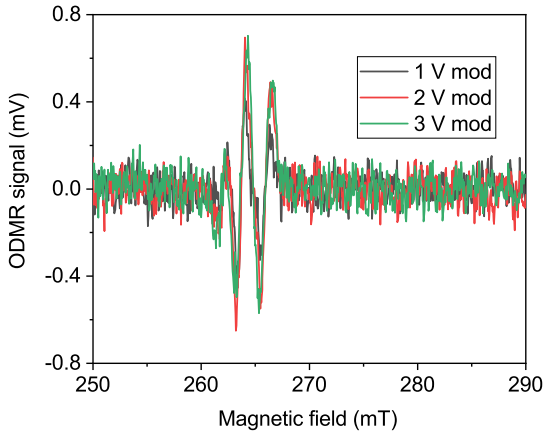

Figure 3. Frequency modulated and magnetic field swept ODMR measurement at 9.2 GHz on NV centers in diamond detected at 680 nm. Note that the derivative Lorentzian lineshapes are due to the frequency modulation similar to magnetic field modulation found in conventional electron spin resonance spectrometers.

Gain = 26 dB). This detection method is essentially the same as if it was a conventional electron spin resonance but the signal is detected optically. The principle of detection is that the microwave field is frequency modulated using the lock-in amplifiers' local oscillator as a sine source connected to the microwave oscillator. In Figure 3, the intensity of such ODMR signal is examined as the amplitude of the modulating sine wave increases. The modulation depth was set to 6 MHz V^{-1} meaning a maximum deviation of 18 MHz in this measurement, however, above 2 V, no significant increase in the ODMR amplitude can be seen.

Figure 4 shows individual ODMR spectra combined together to form a so-called ODMR map. This closely resembles emission–excitation maps used in photoluminescence (PL), with the exception that one axis is the microwave frequency, whereas the other is the wavelength of the emitted light. This measurement was conducted in zero external magnetic field in the form of wavelength sweeps at fixed MW frequency. Here, the microwave sweeper is set to continuous-wave mode and wavelength-resolved PL is recorded as the grating of the spectrometer is rotated. In our setup, we simultaneously detect the DC voltage (the PL signal) and the AC component (the signal detected by the lock-in amplifier) which is the ODMR signal.

The measurement time is determined by the required resolution and range in wavelength and microwave frequency and the integration time. The map shown in Figure 4 was recorded with a 0.5 nm wavelength resolution and a 100 ms integration time. The microwave frequency resolution is 2 MHz in the middle and was changed in bigger steps (10–50 MHz) moving away from the resonance resulting in 45 different values. Altogether, this results in a measurement time of 52.5 min.

3.2. μ-PCD on Silicon Wafers

Figure 5 shows the μ-PCD (or the μ-PCD signal) measured on a phosphorus-doped silicon sample at room temperature and at 77 K. The signal magnitude was obtained from the square root of the squared sum of the I and Q components. The CPW can be readily adapted to cryostat experiments as it can be conveniently

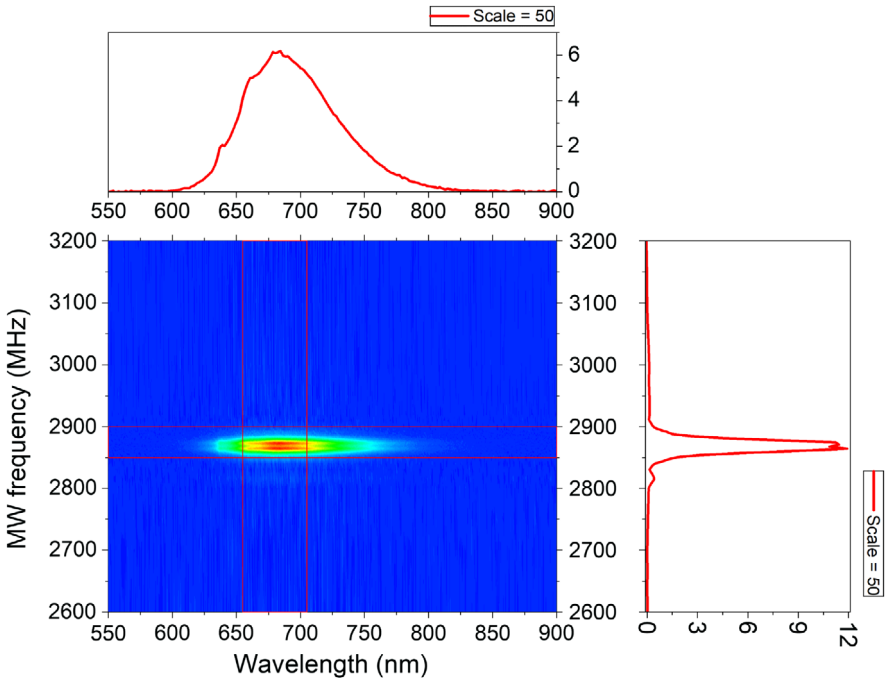

Figure 4. ODMR map. The upper panel is the wavelength-resolved microwave frequency averaged (taken in the range 2849–2899 MHz) PL similar to the well-known PL spectrum of NV centers. The right panel shows a vertical profile cross section (taken in the range 655–705 nm), which corresponds to the microwave frequency-resolved ODMR signal.

© 2020 The Authors. Published by Wiley-VCH GmbH

15213951, 2020, 12, Downloaded from https://onlinelibrary.wiley.com/doi/10.1002/pssb.202000298 by Cochrane Germany, Wiley Online Library on [02/12/2023]. See the Terms and Conditions (https://onlinelibrary.wiley.com/terms-and-conditions) on Wiley Online Library for rules of use; OA articles are governed by the applicable Creative Commons License

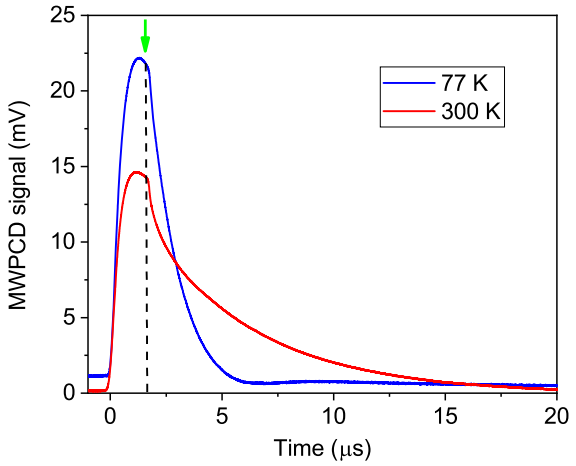

Figure 5. μ-PCD measurement conducted on phosphorus-doped silicon. Red line shows the decay at room temperature and the blue spectrum was recorded at 77 K. The green arrow and the dashed line indicate the end of the laser pulse.

placed on the cold finger of an arbitrary cryostat. In contrast, a microwave resonator usually suffers from a change in the resonant frequency (and the quality factor) as a function of the temperature which affects the measurement sensitivity and also care is required to tune the source frequency to that of the resonator eigenfrequency. The CPW design is free from all these complications.

In case of time-resolved microwave detection, the use of microwave resonators is also impractical as the resonator bandwidth (typically, 100 kHz–1 MHz) significantly limits the available time resolution.[23] The typical power to microwave field conversion is $2.17 \times 10^{-12}\,T^2\,W^{-1}$ for a TE011 type cylindrical cavity. Following the calculations presented in the study by Simons and Arora[24] for our CPW with gaps of 250 μm separated by 1400 μm and a total width of 6 mm, this factor is $0.88 \times 10^{-8}\,T^2\,W^{-1}$. This means that the CPW performs as a cavity with a Q-factor of 4000.

As shown in Figure 5, the cooling leads to shortening of charge carrier lifetime in the investigated material. This is described by the Shockley–Read–Hall theory.[25] The impurities introduce empty gap states, thus giving a rise to recombination. However, these levels can be occupied by thermally excited electrons. With decreasing temperature, fewer states are occupied therefore more recombination centers are present in the sample and the optically excited electrons have a shorter lifetime.

4. Conclusion

We presented the development of an ODMR spectrometer and a microwave photoconductivity decay measurement setup. Both instrument benefit from the CPW structure, namely, the easy optical access to the sample compared to classical microwave resonators and the broadband operation. Low-temperature μ-PCD measurements reveal decreasing carrier lifetime as the silicon sample is cooled. We pointed out that in specific cases, resonators can outperform CPWs in terms of accuracy and sensitivity, but their advantage turns out to be a disadvantage when one needs to change measurement parameters such as microwave frequency or sample temperature. The fast μ-PCD setup can reveal information on charge carrier dynamics in intensively studied novel photovoltaic materials such as methylammonium halide perovskites.

Acknowledgements

This work was supported by the Hungarian National Research, Development and Innovation Office (NKFIH) grant nos. K119442 and 2017-1.2.1-NKP-2017-00001 and by the National Research, Development and Innovation Fund of the Hungarian Government grant no. NVKP_16-1-2016-0018. The research reported in this paper and carried out at BME has been supported by the NRDI Fund (TKP2020 IES, grant no. BME-IE-NAT) based on the charter of bolster issued by the NRDI Office under the auspices of the Ministry for Innovation and Technology.

Conflict of Interest

The authors declare no conflict of interest.

Keywords

coplanar waveguides, microwave-detected photoconductivity decay, nitrogen-vacancy centers, optically detected magnetic resonance

Received: June 3, 2020
Revised: October 1, 2020
Published online: October 26, 2020

[1] M. C. Fischer, J. W. Wilson, F. E. Robles, W. S. Warren, *Rev. Sci. Instrum.* **2016**, *87*, 031101.
[2] C. Lee, T. Rohwer, E. J. Sie, A. Zong, E. Baldini, J. Straquadine, P. Walmsley, D. Gardner, Y. S. Lee, I. R. Fisher, N. Gedik, *Rev. Sci. Instrum.* **2020**, *91*, 043102.
[3] *EPR of Free Radicals in Solids* (Eds: A. Lund, M. Shiotani), Springer, Dordrecht **2003**.
[4] D. Stich, F. Späth, K. Hannes, A. Sperlich, V. Dyakonov, T. Hertel, *Nat. Photonics* **2014**, *8*, 139.
[5] P. A. Lane, L. S. Swanson, Q. X. Ni, J. Shinar, J. P. Engel, T. J. Barton, L. Jones, *Phys. Rev. Lett.* **1992**, *68*, 887.
[6] A. Gruber, A. Dräbenstedt, C. Tietz, L. Fleury, J. Wrachtrup, C. von Borczyskowski, *Science* **1997**, *276*, 2012.
[7] P. Neumann, R. Kolesov, V. Jacques, J. Beck, J. Tisler, A. Batalov, L. Rogers, N. B. Manson, G. Balasubramanian, F. Jelezko, J. Wrachtrup, *New J. Phys.* **2009**, *11*, 013017.
[8] W. Harneit, C. Meyer, A. Weidinger, D. Suter, J. Twamley, *Phys. Status Solidi B* **2002**, *233*, 453.
[9] J. Shinar, *Laser Photonics Rev.* **2012**, *6*, 767.
[10] J. Wrachtrup, C. von Borczyskowski, J. Bernard, M. Orrit, R. Brown, *Phys. Rev. Lett.* **1993**, *71*, 3565.
[11] M. Kunst, G. Beck, *J. Appl. Phys.* **1986**, *60*, 3558.
[12] B. Berger, N. Schüler, S. Anger, B. Gründig-Wendrock, J. R. Niklas, K. Dornich, *Phys. Status Solidi A* **2011**, *208*, 769.
[13] G. F. Novikov, A. A. Marinin, E. V. Rabenok, *Instrum. Exp. Techn.* **2010**, *53*, 83.
[14] K. Sasaki, Y. Monnai, S. Saijo, R. Fujita, H. Watanabe, J. Ishi-Hayase, K. M. Itoh, E. Abe, *Rev. Sci. Instrum.* **2016**, *87*, 053904.
[15] C. P. Wen, *IEEE Trans. Microw. Theory Tech.* **1969**, *17*, 1087.

© 2020 The Authors. Published by Wiley-VCH GmbH

15213951, 2020, 12, Downloaded from https://onlinelibrary.wiley.com/doi/10.1002/pssb.202000298 by Cochrane Germany, Wiley Online Library on [02/12/2023]. See the Terms and Conditions (https://onlinelibrary.wiley.com/terms-and-conditions) on Wiley Online Library for rules of use; OA articles are governed by the applicable Creative Commons License

[16] W. Jia, Z. Shi, X. Qin, X. Rong, J. Du, *Rev. Sci. Instrum.* **2018**, *89*, 064705.
[17] S. B. Cohn, *IEEE Trans. Microw. Theory Tech.* **1969**, *17*, 768.
[18] R. Simons, *Coplanar Waveguide Circuits, Components, and Systems*, Wiley, New York **2002**.
[19] F. Gustrau, *RF and Microwave Engineering*, Wiley, Hoboken, NJ **2012**.
[20] S. Yamamoto, K. Shitamitsu, H. Kurisu, M. Matsuura, K. Oshiro, H. Mikami, S. Fujii, *Phys. Status Solidi B* **2004**, *241*, 1769.
[21] S. G. Cho, J. Kim, I. Kim, K. H. Kim, M. Yamaguchi, *Phys. Status Solidi A* **2007**, *204*, 4133.
[22] L. Yuan, Z. Yue, S. Meng, L. Li, *Phys. Status Solidi A* **2014**, *211*, 1828.
[23] B. Gyüre-Garami, B. Blum, O. Sági, A. Bojtor, S. Kollarics, G. Csősz, B. G. Márkus, J. Volk, F. Simon, *J. Appl. Phys.* **2019**, *126*, 235702.
[24] R. N. Simons, R. K. Arora, *IEEE Trans. Microw. Theory Tech.* **1982**, *30*, 1094.
[25] R. N. Hall, *Phys. Rev.* **1952**, *87*, 387.

© 2020 The Authors. Published by Wiley-VCH GmbH

15213951, 2020, 12, Downloaded from https://onlinelibrary.wiley.com/doi/10.1002/pssb.202000298 by Cochrane Germany, Wiley Online Library on [02/12/2023]. See the Terms and Conditions (https://onlinelibrary.wiley.com/terms-and-conditions) on Wiley Online Library for rules of use; OA articles are governed by the applicable Creative Commons License